Article

Not peer-reviewed version

Automated Detection of *Amaranthus palmeri* in Crops of the Brazilian Cerrado Using RPA Images and Deep Learning

Denilson Pereira Passo *, Rodrigo Rodrigues Antunes, Edilson de Souza Bias, Gilson Alexandre Ostwald Pedro da Costa, Raul Queiroz Feitosa, Thanan Walesza Pequeno Rodrigues, Omar Roberto da Silveira

Posted Date: 24 April 2026

doi: 10.20944/preprints202604.1707.v1

Keywords: *Amaranthus palmeri*; deep learning; YOLO; weed detection; remotely piloted aircraft; Cerrado; object detection; precision agriculture

 doi:10.20944/preprints202604.1707.v1

Article

Automated Detection of *Amaranthus palmeri* in Crops of the Brazilian Cerrado Using RPA Images and Deep Learning

Denilson Pereira Passo [1,*], Rodrigo Rodrigues Antunes [1], Edilson de Souza Bias [1], Gilson Alexandre Ostwald Pedro da Costa [2], Raul Queiroz Feitosa [3], Thanan Walesza Pequeno Rodrigues [4] and Omar Roberto da Silveira [5]

[1] Department of Geosciences, University of Brasília, Brasília 70910-900, DF, Brazil
[2] Department of Computer Science, Rio de Janeiro State University, Rio de Janeiro 20550-013, RJ, Brazil
[3] Pontifical Catholic University of Rio de Janeiro, Rio de Janeiro 22451-900, RJ, Brazil
[4] Federal Institute of Brasília, Campus Riacho Fundo, Brasília 71805-772, DF, Brazil
[5] Ministry of Agriculture and Livestock, Federal Superintendence of Agriculture, Cuiabá 78043-400, MT, Brazil
* Correspondence: geodenilson@gmail.com

Abstract

Amaranthus palmeri has become established in agricultural areas of the Brazilian Cerrado, where it threatens soybean and cotton yields. Conventional field scouting cannot cover the large properties typical of the region fast enough to detect infestation foci before seed set. We tested an automated detection approach using aerial images from a remotely piloted aircraft (RPA), a DJI Matrice 300 RTK with a Zenmuse P1 camera (45 megapixels, MP), processed with YOLOv11x (You Only Look Once, version 11, extra-large). Four field campaigns in Sapezal, Mato Grosso, produced roughly 40,000 images over soybean and cotton at different weed growth stages; flight tests at 90, 20, and 12 m showed that 12–20 m altitude is needed to resolve individual plants. Two specialists annotated 382 *Amaranthus* individuals (*A. palmeri* and *A. hybridus*), split 70/30 for training and validation. Overall performance reached 84% precision, 84% recall, and 88% mean average precision at Intersection-over-Union 0.5 (mAP@0.5); for *A. palmeri* alone the figures were 95%, 93%, and 99%, respectively, with 98% accuracy in the confusion matrix and virtually no cross-class confusion. Within these limits, RPA imagery and deep learning can replace manual scouting for *A. palmeri* at the farm scale.

Keywords: *Amaranthus palmeri*; deep learning; YOLO; weed detection; remotely piloted aircraft; Cerrado; object detection; precision agriculture

1. Introduction

Invasive plant species affect crop productivity, native biodiversity, and public health worldwide [1]. Among them, *Amaranthus palmeri* (Palmer amaranth), native to the southwestern United States and northern Mexico [2–4], stands out because of documented yield losses exceeding 90% in maize and 79% in soybean under heavy infestation [4–7,14]. Its presence in a field also drives up herbicide use, raising production costs and environmental exposure [5,8,9].

The genus *Amaranthus* (Amaranthaceae) includes about 75 species [2]; the two that cause the most agronomic damage through herbicide resistance are *A. tuberculatus* and *A. palmeri* [10]. Murphy and Tranel [11] developed species-specific SNP markers for these and other weedy amaranths (*A. hybridus*, *A. powellii*, *A. retroflexus*, among others). *A. palmeri* is dioecious, glabrous, with erect branched stems and panicle-type inflorescences [12]. It grows 25–50 mm day^{-1} and a single plant can produce 100,000–500,000 seeds [12–14], which explains why even a few missed individuals in a field can lead to rapid re-infestation. Barroso et al. [15] attribute this competitive dominance to a C_4 photosynthetic rate, efficient water use, and fast biomass accumulation. The plant is also toxic to cattle through

 doi:10.20944/preprints202604.1707.v1

nitrate accumulation in the leaves [14]. Populations resistant to acetolactate synthase (ALS) inhibitors, 5-enolpyruvylshikimate-3-phosphate synthase (EPSPS) inhibitors, and, more recently, glufosinate have been confirmed in several countries [7,9,16–18].

Records of *A. palmeri* now span China [7], Europe [20], and South America, where it was first documented in Argentina in 1984 [19]. Ferreira et al. [21] modeled its potential distribution under current and future climate scenarios, indicating favorable conditions for further spread. In Brazil, official detection occurred in 2015 in the state of Mato Grosso [9,12,15,22,23]. Molecular studies by Gazziero et al. [23] indicated that Brazilian biotypes are genetically more similar to North American populations than to Argentine ones, suggesting introduction via used combines imported from the United States. Subsequent dispersal has been facilitated by the movement of agricultural machinery between farms, prompting states such as Goiás, Tocantins, and the Federal District to be on alert [23,24]. Netto et al. [9] documented multiple resistance to ALS and EPSPS inhibitors in Mato Grosso, and the number of herbicide-resistant weed species continues to increase worldwide [25].

On Cerrado farms that can span tens of thousands of hectares, detecting *A. palmeri* foci before the plants set seed is the single most cost-effective management action, but walking those areas is not feasible. Remotely piloted aircraft (RPAs) with high-resolution cameras now make large-area surveys practical; the bottleneck, however, has shifted to data interpretation, because manually inspecting thousands of images per flight is not viable. Convolutional neural network (CNN) detectors address this by learning to locate and classify objects directly from pixel data, bypassing the hand-crafted feature pipelines required by Random Forest [13,26] and maximum-likelihood classifiers [16]. The YOLO (You Only Look Once) family [27,28] is well suited to this task because it processes each image in a single forward pass. Its latest iteration, YOLO11 [29,30], adds spatial attention blocks to the convolutional backbone, which helps localize small objects such as individual weed plants in dense canopy backgrounds.

Published work on *Amaranthus* detection by remote sensing is concentrated in North America and Europe. Early efforts relied on object-based image analysis (OBIA) applied to RPA imagery [31] or on supervised classification of multispectral data, as in the work of Sanders et al. [16], who achieved 80–90% overall accuracy for discriminating *A. palmeri* from soybean in a two-class setting. Hyperspectral approaches have also been explored: Fletcher and Turley [13] separated *A. palmeri* from colored cotton with 78–89% accuracy using canopy spectroradiometer data, while Basinger et al. [32] showed that spectral differentiation between *A. palmeri* and *Digitaria sanguinalis* is inconsistent across years and growth stages. At UAV scale, De Castro et al. [26] combined Random Forest with OBIA to map weeds in sunflower and cotton fields, reaching weed detection accuracy of up to 88%. A common limitation across these studies is the dependence on multispectral or hyperspectral sensors and the restriction to North American or European field conditions. The Brazilian Cerrado presents a different combination of soil color, solar angle, crop spacing, and weed community composition, and no study has tested deep learning object detection on *A. palmeri* in this biome.

This paper tests whether YOLOv11x [29] can detect *A. palmeri* in aerial RGB images collected at 12–20 m altitude over cotton fields in Sapezal, Mato Grosso. The trained model was integrated into the open-source GeoLearning plugin for QGIS [34], whose architecture is described separately.

2. Materials and Methods

The work had two phases: field data collection (equipment selection, flight planning, image acquisition, GPS ground-truthing) and model development (annotation, training, and evaluation).

2.1. Study Area

Fieldwork took place in Sapezal (13°32′33″ S; 58°48′51″ W), 670 km from Cuiabá, Mato Grosso, Brazil. The municipality is one of the largest soybean and cotton producers in the country, and *A. palmeri* has been confirmed there since at least 2015. We chose this site because it offered fields under both crops at different weed growth stages within driving distance of each other, which simplified logistics during the four expeditions.

 doi:10.20944/preprints202604.1707.v1

2.2. Image Acquisition by RPA

The aerial images were obtained using a DJI Matrice 300 RTK drone equipped with a DJI Zenmuse P1 camera (45-megapixel sensor, DL 35 mm F2.8 LS ASPH lens) during four field expeditions conducted between November 2024 and May 2025 in the Sapezal region. Six flight missions were conducted over soybean and cotton fields with a confirmed presence of *Amaranthus* spp., at altitudes between 12 and 20 m and with 80% overlap. According to the camera specifications, the ground sample distance (GSD) at 12 m altitude is approximately 0.15 cm pixel^{-1} and at 20 m approximately 0.25 cm pixel^{-1}, providing sub-centimetric spatial resolution suitable for individual plant discrimination.

In total, roughly 40,000 photographs were acquired: 7940 over soybean, 5339 over cotton with a predominance of *A. palmeri*, and 7428 over cotton with a predominance of *A. hybridus*. We also collected 250 ground control points with an RTK GPS receiver, tagging each with the *Amaranthus* species identified on site.

2.3. Training Data

From the full image collection, we selected photographs taken over cotton fields that contained visible *Amaranthus* individuals. Selection favored diversity in lighting, weed density, and position relative to the crop rows. Each original frame was 5472 $\times$ 3648 pixels.

Soybean fields were also overflown, but those images turned out to be unusable: the flights were the team's first with this equipment, and the altitude was set too high for the required GSD. By the time we had calibrated the flight parameters on the later cotton campaigns, the soybean season had ended and the 1200 km round trip from Brasília to Sapezal made a return visit impractical. As a result, all annotated data come from cotton fields.

Two specialists annotated the images independently using bounding boxes in the YOLO format, labeling each plant as either *A. palmeri* or *A. hybridus*. Disagreements (roughly 8% of the annotations) were reviewed jointly and resolved before the dataset was finalized. In total, 382 plants were identified and annotated. The dataset was split into 267 samples (70%) for training and 115 samples (30%) for validation, a standard split in the computer vision literature.

2.4. Model Architecture

We used YOLOv11x [29,30], the largest variant in the YOLO11 family. Preliminary tests with lighter variants (YOLOv11s and YOLOv11m) showed that they missed smaller *Amaranthus* individuals, particularly those partially hidden by cotton leaves; the extra depth of the "x" variant was needed to capture those subtle morphological cues.

YOLO11 extends previous YOLO versions by adding spatial attention mechanisms to the convolutional pipeline [29]. It is organized into three components:

- **Backbone**: extracts features from the input image at multiple scales using C3k2 blocks (a compact version of the Cross Stage Partial bottleneck with two smaller convolutions), the Spatial Pyramid Pooling Fast (SPPF) module for multi-scale feature aggregation, and a Cross Stage Partial with Spatial Attention (C2PSA) block that enables the network to focus on visually relevant regions.
- **Neck**: aggregates and refines multi-scale features using C3k2 blocks, preserving both fine details (e.g., leaf shape) and contextual information (e.g., spatial arrangement in the field).
- **Head**: generates bounding box coordinates and classification probabilities through C3k2 blocks followed by optimized convolutional layers.

Training began from pre-trained weights on the COCO dataset [33], using fine-tuning to adapt to the specific characteristics of the problem.

2.5. Training Procedure

Images were resized to 1024 $\times$ 1024 pixels. We tested 640 px initially but found that smaller *A. hybridus* individuals became too blurred to annotate cleanly, so we moved to the higher resolution

 doi:10.20944/preprints202604.1707.v1

despite the increased memory cost. Batch size was 16; larger batches exceeded the free-tier GPU memory on Google Colab.

Training ran for up to 1000 epochs with early stopping after 100 epochs of no improvement in validation mAP@0.5. Automatic Mixed Precision (AMP) was enabled to keep the training within the memory budget of the Colab T4 GPU.

2.6. Data Augmentation

Field images vary widely in lighting, viewing angle, plant density, and soil moisture. To prevent the model from overfitting to the limited training set, we applied the following augmentation pipeline:

- **Mosaic**: combination of four images into a single composition, applied to 100% of the samples during training, except in the last 10 epochs, when it is disabled to allow fine-tuning of the weights;
- **Geometric transformations**: horizontal flipping (50% probability), scale variation (up to $\pm$50%) and translation (up to $\pm$10%);
- **Photometric transformations**: random variations in hue (up to 1.5%), saturation (up to 70%) and brightness (up to 40%);
- **Random erasing**: random occlusion of rectangular regions in 40% of the samples, simulating partial obstructions by crop leaves or shadows.

With only 267 training images, augmentation was not optional; without it, the model overfitted within the first 50 epochs in our preliminary runs.

2.7. Evaluation Metrics

Performance was assessed on the 115-sample validation set using precision (P), recall (R), and mean average precision at an Intersection-over-Union threshold of 0.5 (mAP@0.5). The normalized confusion matrix was also computed to identify systematic misclassifications between the two *Amaranthus* classes and the background.

3. Results

3.1. Training Overview

Early stopping halted training at epoch 298. The loss curves showed steady convergence up to around epoch 180, after which improvements became marginal. Validation losses stabilized slightly above training losses, with no divergence indicative of overfitting. Given the small annotation set (382 plants), this behavior was better than expected; we attribute it largely to the mosaic augmentation, which effectively multiplied the number of scene compositions the model saw during training.

3.2. Overall and Per-Class Performance

Table 1 presents the performance metrics obtained on the validation set at the best checkpoint.

Table 1. Detection performance metrics per class on the validation set.

Class	Precision	Recall	mAP@0.5
All (global)	0.84	0.84	0.88
A. palmeri	0.95	0.93	0.99
A. hybridus	0.74	0.75	0.77

An overall precision and recall of 84% each means roughly one in six detections is a false positive, and one in six real plants is missed. In a phytosanitary context, the false-negative rate is the more worrisome figure, since each undetected plant can produce hundreds of thousands of seeds. At the current recall level, a follow-up targeted field check of flagged areas would still be advisable, but the model eliminates the need to walk entire fields.

 doi:10.20944/preprints202604.1707.v1

The Precision–Recall curves (Figure 1) show the relationship between precision and recall for each class. The mAP@0.5 of 88% confirms adequate overlap between predicted and reference bounding boxes. Performance differed markedly between classes: *A. palmeri* reached mAP@0.5 of 99%, while *A. hybridus* reached 77%. The lower score for *A. hybridus* likely reflects both the greater morphological variability of this group (which may include natural hybrids with other *Amaranthus* species) and a smaller number of annotated samples compared with *A. palmeri* in the training set.

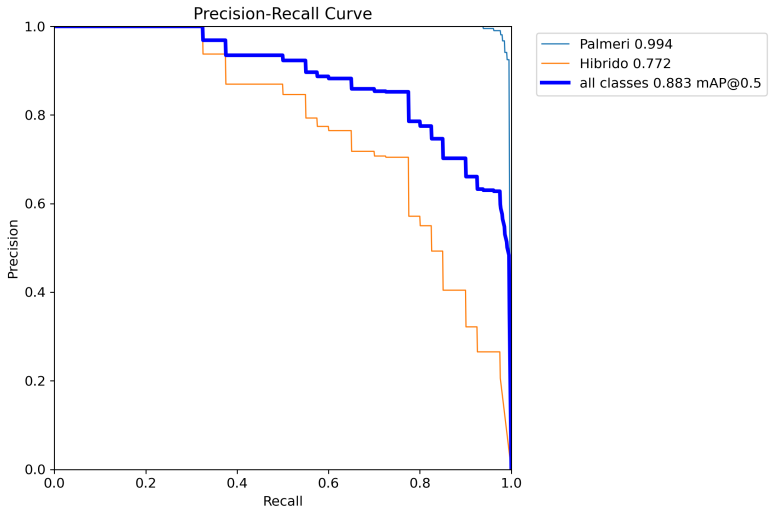

Figure 1. Precision–Recall curves for each class and the global average.

3.3. Confusion Matrix Analysis

The normalized confusion matrix (Figure 2) breaks down where the model gets things right and where it fails. *A. palmeri* was correctly classified in 98% of the cases; the remaining 2% were labeled as background, typically in images where a plant was at the very edge of the frame. The high accuracy for this species likely reflects its distinctive upright inflorescence, which produces a recognizable shape and shadow pattern even at sub-centimetric resolution.

Figure 2. Normalized confusion matrix for the validation set.

 doi:10.20944/preprints202604.1707.v1

The *A. hybridus* class reached 82% accuracy, with 17% false negatives. We suspect the main source of misses is occlusion: smaller hybrid plants are often partially covered by cotton leaves and, at that point, the remaining visible pixels look very similar to the crop background. During annotation we noticed that even the human specialists hesitated on several of these borderline cases. More training samples of *A. hybridus* at early growth stages would likely help, but reducing occlusion-related errors may ultimately require segmentation masks rather than bounding boxes.

Cross-class confusion between the two species was virtually zero, which is the result that matters most for management: if the model flags a plant as *A. palmeri*, the agronomist can act on that label without needing a secondary verification step in the field.

4. Discussion

4.1. Comparison with Previous Work

Table 2 places our results alongside related studies. The comparison is imperfect because the studies use different sensors, classifiers, species, and evaluation protocols, but the side-by-side view highlights where our approach sits relative to the state of the art.

Table 2. Comparison with related weed detection studies. OA = overall accuracy; WdA = weed detection accuracy.

Study	Method	Sensor	Target	Best Reported Metric
Sanders et al. [16]	Supervised classification	Multispectral (5-band, UAV)	*A. palmeri* in soybean	OA: 80–90% (2-class)
Fletcher and Turley [13]	Random Forest (cforest)	Hyperspectral (spectroradiometer)	*A. palmeri* vs. cotton	OA: 77.8–88.9%
De Castro et al. [26]	RF-OBIA	RGNIR (UAV)	Weeds in sunflower/cotton	R^2: 0.57–0.91; WdA: 59–88%
Basinger et al. [32]	Spectral analysis	Hyperspectral (in-situ)	*A. palmeri*, *D. sanguinalis*	Differentiation at $P \leq 0.1$
This study	YOLOv11x (deep learning)	RGB (45 MP, UAV)	*A. palmeri* in cotton	mAP@0.5: 0.88 (global); 0.99 (*A. palmeri*)

The most directly comparable study is that of Sanders et al. [16], who reached 80–90% overall accuracy in a two-class discrimination of *A. palmeri* versus soybean using a five-band multispectral sensor. When they expanded the problem to eight classes (adding weed density levels), accuracy collapsed to 12–35%, a result that exposes the ceiling of conventional supervised classifiers on complex scenes. Fletcher and Turley [13] obtained 78–89% accuracy for separating *A. palmeri* from colored cotton, but relied on laboratory-grade hyperspectral measurements and still suffered from cotton pixels being mislabeled as weed. The RF-OBIA approach of De Castro et al. [26] detected weeds in sunflower and cotton with up to 88% accuracy (R^2 up to 0.91 for weed coverage), though at a coarser 30 m flight altitude. A common thread across these studies is the dependence on spectral information beyond RGB. Basinger et al. [32] made this explicit by showing that hyperspectral differentiation between *A. palmeri* and *D. sanguinalis* breaks down across years and growth stages, raising questions about the long-term reliability of purely spectral approaches.

Our approach departs from these precedents in two concrete ways. First, YOLOv11x learns its own feature representations from RGB data, which removes the need for multispectral or hyperspectral hardware and the associated calibration overhead. Second, the model was trained and validated on images collected under Brazilian Cerrado conditions (red-orange latosol background, tropical lighting, narrow-row cotton at 0.76 m spacing), rather than transferred from North American or European datasets. Whether these Cerrado-specific patterns transfer to other tropical regions remains untested.

4.2. Cost–Benefit Considerations

The dataset was built with a DJI Matrice 300 RTK and a Zenmuse P1 camera, equipment that costs tens of thousands of USD. We needed that level of quality for annotation: at coarser resolutions,

 doi:10.20944/preprints202604.1707.v1

the annotators could not confidently delineate individual plants. The trained model, however, does not require the same platform at inference time. Any RPA that delivers a GSD fine enough to resolve individual plants (roughly ≤ 0.3 cm) can supply usable input. We have not yet formally tested the model on imagery from lower-cost drones (e.g., DJI Mavic series), but the architecture operates on pixel patterns, not on sensor metadata, so the transfer should hold as long as the spatial resolution is adequate.

Training was done on Google Colab using a free-tier GPU; the full 298-epoch run took approximately 4 h. The trained model runs inside the GeoLearning plugin for QGIS [34], which is free and open-source. On a typical Cerrado farm exceeding 10,000 ha, deploying one or two drone flights per critical growth window is far cheaper than sending scouts on foot. Cooperative equipment-sharing and drone-as-a-service providers, already common in the region for spraying, could further reduce costs.

4.3. Limitations

All validation images come from cotton fields near Sapezal, Mato Grosso. Soybean imagery was collected during the first field campaigns but proved unusable because the flight altitude had not yet been calibrated for the necessary GSD; logistical constraints (round trips of over 1200 km from Brasília) prevented a second attempt during the soybean season. How the model behaves on soybean, maize, or other crop backgrounds is therefore unknown at this point.

With 382 annotated plants, the dataset is small by computer vision standards. It is adequate for a proof of concept but far from sufficient to claim robustness across the full range of phenological stages, lighting conditions, and soil types found in the Cerrado. The annotation bottleneck is not computational but human: each bounding box was reviewed by two specialists, and scaling this process requires either more personnel or semi-automated pre-labeling.

The two-class scheme (*A. palmeri* vs. *A. hybridus*) ignores other *Amaranthus* species and broadleaf weeds that co-occur in the same fields. In practice, a grower needs to know whether a detected plant warrants a specific herbicide or just general management. Adding more classes will demand not only more data but also clearer taxonomic ground-truthing, which is non-trivial given the morphological overlap within the genus.

5. Conclusions

A YOLOv11x model trained on 382 annotated *Amaranthus* plants from aerial RGB images over cotton fields in Sapezal, Mato Grosso, achieved 88% mAP@0.5 overall and 99% for *A. palmeri*. The normalized confusion matrix showed 98% accuracy for the target species and virtually zero cross-class confusion between *A. palmeri* and *A. hybridus*. These numbers were obtained with a relatively small dataset and a standard RGB camera, which suggests that further gains are within reach as more annotated data become available.

From a practical standpoint, the model already runs inside the open-source GeoLearning plugin for QGIS [34] and can process drone imagery without specialized spectral sensors. For Cerrado farms, where individual properties often exceed 10,000 ha, automated aerial screening is the only realistic way to detect *A. palmeri* foci before they set seed and spread through machinery traffic. The architecture and functionalities of the plugin are detailed in a companion publication, and the annotated dataset will be publicly released alongside a separate article currently under review (Antunes et al., submitted).

The main bottleneck going forward is the annotation effort. Expanding coverage to soybean and maize backgrounds, adding samples from other Cerrado regions, and including more weed species are all necessary, but each requires field campaigns and expert labeling time. Integration with variable-rate spraying systems is another logical step, though it will require testing the model's reliability under the faster processing constraints of real-time field applications.

Author Contributions: Conceptualization, D.P.P. and E.S.B.; methodology, D.P.P. and R.R.A.; software, R.R.A.; validation, D.P.P., R.R.A. and O.R.S.; formal analysis, D.P.P.; investigation, D.P.P. and O.R.S.; resources, E.S.B. and

 doi:10.20944/preprints202604.1707.v1

O.R.S.; data curation, D.P.P. and R.R.A.; writing—original draft preparation, D.P.P.; writing—review and editing, G.A.O.P.C., R.Q.F. and T.W.P.R.; visualization, D.P.P.; supervision, E.S.B. and G.A.O.P.C.; project administration, E.S.B.; funding acquisition, E.S.B. All authors have read and agreed to the published version of the manuscript.

Funding: This research was funded by the Federal District Research Support Foundation (FAP-DF) and the Coordination for the Improvement of Higher Education Personnel (CAPES).

Institutional Review Board Statement: Not applicable.

Informed Consent Statement: Not applicable.

Data Availability Statement: The data presented in this study are openly available in Zenodo at https://doi.org/10.5281/zenodo.19668941, reference number 10.5281/zenodo.19668941, under a Creative Commons Attribution 4.0 International (CC-BY 4.0) license. The dataset contains annotated aerial RGB images of *Amaranthus palmeri* and *A. hybridus* with YOLO-format bounding-box annotations and the corresponding `data.yaml` configuration file. The dataset is described in detail in a companion data descriptor (Antunes et al., submitted). The trained YOLOv11x model weights are available from the corresponding author upon reasonable request.

Acknowledgments: The authors thank the partner farms in the Sapezal-MT region for granting access to the study areas and the Secretariat of Agriculture, Supply and Rural Development of the Federal District (SEAGRI-DF) for its institutional support.

Conflicts of Interest: The authors declare no conflicts of interest. The funders had no role in the design of the study; in the collection, analyses, or interpretation of data; in the writing of the manuscript; or in the decision to publish the results.

Abbreviations

The following abbreviations are used in this manuscript:

ALS	Acetolactate synthase
AMP	Automatic Mixed Precision
C2PSA	Cross Stage Partial with Spatial Attention
CNN	Convolutional neural network
COCO	Common Objects in Context
EPSPS	5-Enolpyruvylshikimate-3-phosphate synthase
GSD	Ground sample distance
IoU	Intersection over Union
mAP	Mean average precision
OBIA	Object-based image analysis
RPA	Remotely piloted aircraft
SPPF	Spatial Pyramid Pooling Fast
YOLO	You Only Look Once

References

1. Fenner, M. Ecology of invasive plants. In *Encyclopedia of Ecology*; Elsevier: Amsterdam, The Netherlands, 2008; pp. 1153–1159.
2. Ward, S.M.; Webster, T.M.; Steckel, L.E. Palmer amaranth (*Amaranthus palmeri*): A review. *Weed Technol.* **2013**, *27*, 12–27. https://doi.org/10.1614/WT-D-12-00113.1
3. Sauer, J.D. Recent migration and evolution of the dioecious amaranths. *Evolution* **1957**, *11*, 11–31. https://doi.org/10.1111/j.1558-5646.1957.tb02872.x
4. Borgato, E.A.; Ohadi, S.; Brunharo, C.A.C.G.; Patterson, E.L.; Matzrafi, M. *Amaranthus palmeri* S. Watson reproduction system: Implications for distribution and management strategies. *Weed Res.* **2025**, *65*, e12626. https://doi.org/10.1111/wre.12626
5. Carvalho, S.J.P.; Gonçalves Netto, A.; Nicolai, M.; Cavenaghi, A.L.; López-Ovejero, R.F.; Christoffoleti, P.J. Detection of glyphosate-resistant Palmer amaranth (*Amaranthus palmeri*) in agricultural areas of Mato Grosso, Brazil. *Planta Daninha* **2015**, *33*, 579–586. https://doi.org/10.1590/S0100-83582015000300020

 doi:10.20944/preprints202604.1707.v1

6. Oliveira, M.C.; Jhala, A.J.; Bernards, M.L.; Proctor, C.A.; Stepanovic, S.; Werle, R. Palmer amaranth (*Amaranthus palmeri*) adaptation to US Midwest agroecosystems. *Front. Agron.* **2022**, *4*, 887629. https://doi.org/10.3389/fagro.2022.887629
7. Jiao, X.; Long, M.; Li, J.; Yang, Q.; Liu, Z. Reconstructing the invasive history and potential distribution prediction of *Amaranthus palmeri* in China. *Agronomy* **2023**, *13*, 2498. https://doi.org/10.3390/agronomy13102498
8. Gazziero, D.L.P.; Adegas, F.S. *Amaranthus palmeri no Brasil*; Embrapa Soja: Londrina, Brazil, 2016.
9. Gonçalves Netto, A.; Nicolai, M.; Carvalho, S.J.P.; Borgato, E.A.; Christoffoleti, P.J. Multiple resistance of *Amaranthus palmeri* to ALS and EPSPS inhibiting herbicides in the state of Mato Grosso, Brazil. *Planta Daninha* **2016**, *34*, 581–587. https://doi.org/10.1590/S0100-83582016340300019
10. Montgomery, J.S.; Sadeque, A.; Giacomini, D.A.; Brown, P.J.; Tranel, P.J. Sex-specific markers for waterhemp (*Amaranthus tuberculatus*) and Palmer amaranth (*Amaranthus palmeri*). *Weed Sci.* **2019**, *67*, 412–418. https://doi.org/10.1017/wsc.2019.27
11. Murphy, B.P.; Tranel, P.J. Identification and validation of *Amaranthus* species-specific SNPs within the ITS region: Applications in quantitative species identification. *Crop Sci.* **2018**, *58*, 304–311. https://doi.org/10.2135/cropsci2017.06.0359
12. Trezzi, M.M.; von Hertwig Bittencourt, H.; Galon, L.; Diesel, F.; Vidal, R.A. Biological characteristics, resistance to herbicides and management of *Amaranthus palmeri* in agroecosystems. *Rev. Bras. Herbic.* **2016**, *15*, 48–57. https://doi.org/10.7824/rbh.v15i1.429
13. Fletcher, R.S.; Turley, R.B. Employing canopy hyperspectral narrowband data and random forest algorithm to differentiate Palmer amaranth from colored cotton. *Am. J. Plant Sci.* **2017**, *8*, 3258–3271. https://doi.org/10.4236/ajps.2017.812219
14. Hensleigh, P.; Pokorny, M. *Palmer Amaranth (Amaranthus palmeri S. Watson)*; Agronomy Technical Note MT-92; USDA-NRCS Montana: Bozeman, MT, USA, 2017.
15. Barroso, A.A.M.; Hijano, N.; Alves, P.L.C.A. Biologia das plantas daninhas resistentes ao glyphosate no Brasil. *Cerrado Agrociências* **2017**, *8*, 75–87.
16. Sanders, J.T.; Jones, E.A.L.; Austin, R.; Roberson, G.T.; Richardson, R.J.; Everman, W.J. Remote sensing for Palmer amaranth (*Amaranthus palmeri* S. Wats.) detection in soybean (*Glycine max* (L.) Merr.). *Agronomy* **2021**, *11*, 1909. https://doi.org/10.3390/agronomy11101909
17. Carvalho-Moore, P.; Norsworthy, J.K.; González-Torralva, F.; Hwang, J.-I.; Patel, J.D.; Barber, L.T.; Butts, T.R.; McElroy, J.S. Unraveling the mechanism of resistance in a glufosinate-resistant Palmer amaranth (*Amaranthus palmeri*) accession. *Weed Sci.* **2022**, *70*, 370–379. https://doi.org/10.1017/wsc.2022.40
18. Noguera, M.M.; Porri, A.; Werle, I.S.; Heiser, J.; Brändle, F.; Lerchl, J.; Bowe, S.; Asmus, A.; Roma-Burgos, N. Involvement of glutamine synthetase 2 (GS2) amplification and overexpression in *Amaranthus palmeri* resistance to glufosinate. *Planta* **2022**, *256*, 57. https://doi.org/10.1007/s00425-022-03968-2
19. Covas, G. Las especies de *Amaranthus* L. (Amaranthaceae), nativas o naturalizadas en la Provincia de La Pampa. *Apuntes para la Flora de La Pampa* **1984**, *84–86*, 333–341.
20. Matzrafi, M.; Scarabel, L.; Milani, A.; Iamonico, D.; Torra, J.; Recasens, J.; Travlos, I.; Kaczmarek-Derda, W.; Ulber, L.; Stankiewicz-Kosyl, M.; et al. *Amaranthus palmeri* S. Watson: A new threat to agriculture in Europe and the Mediterranean region. *Weed Res.* **2025**, *65*, e12596. https://doi.org/10.1111/wre.12596
21. Ferreira, S.R.; Silva, A.F.D.; Silveira, O.R.D.; Santos, J.C.B.D.; Batista, A.C.; Araújo, F.H.V.; Silva, R.S.D. Potential distribution of *Amaranthus palmeri* under current and future climatic conditions in Brazil and the world. *Adv. Weed Sci.* **2023**, *41*, e020230023. https://doi.org/10.51694/AdvWeedSci/2023;41:00023
22. Andrade Jr., E.R.; Cavenaghi, A.L.; Guimarães, S.C.; Carvalho, S.J.P. *Primeiro relato de Amaranthus palmeri no Brasil em áreas agrícolas no estado do Mato Grosso*; Circular Técnica 19; Instituto Mato-grossense do Algodão (IMAmt): Cuiabá, Brazil, 2015; pp. 1–8.
23. Gazziero, D.L.P.; Silva, A.F.D.; Silveira, O.R.D.; Duke, S.O.; Cerdeira, A.L. Introduction and management of *Amaranthus palmeri* in Brazil. *Adv. Weed Sci.* **2023**, *41*, e020220076. https://doi.org/10.51694/AdvWeedSci/2023;41:00010
24. Brasil. Ministério da Agricultura e Pecuária. *Prevenção e Controle de Amaranthus palmeri*; MAPA: Brasília, Brazil, 2023. Available online: https://www.gov.br/agricultura/pt-br/assuntos/insumos-agropecuarios/insumos-agricolas/agrotoxicos/amaranthus-palmeri (accessed on 20 April 2026).
25. Heap, I. International Survey of Herbicide Resistant Weeds. Available online: http://www.weedscience.org/ (accessed on 5 July 2025).

 doi:10.20944/preprints202604.1707.v1

26. De Castro, A.I.; Torres-Sánchez, J.; Peña, J.M.; Jiménez-Brenes, F.M.; Csillik, O.; López-Granados, F. An automatic random forest-OBIA algorithm for early weed mapping between and within crop rows using UAV imagery. *Remote Sens.* **2018**, *10*, 285. https://doi.org/10.3390/rs10020285
27. Redmon, J.; Divvala, S.; Girshick, R.; Farhadi, A. You only look once: Unified, real-time object detection. In Proceedings of the IEEE Conference on Computer Vision and Pattern Recognition, Las Vegas, NV, USA, 27–30 June 2016; pp. 779–788.
28. Jegham, N.; Koh, C.Y.; Abdelatti, M.; Hendawi, A. YOLO evolution: A comprehensive benchmark and architectural review of YOLOv12, YOLO11, and their previous versions. *arXiv* **2024**, arXiv:2411.00201. https://doi.org/10.48550/arXiv.2411.00201
29. Khanam, R.; Hussain, M. YOLOv11: An overview of the key architectural enhancements. *arXiv* **2024**, arXiv:2410.17725. https://doi.org/10.48550/arXiv.2410.17725
30. Ultralytics. *Ultralytics YOLO11 Documentation and Release Notes*; Version 8.3.0; Ultralytics Inc.: Frederick, MD, USA, 2024. Available online: https://docs.ultralytics.com/models/yolo11/ (accessed on 5 July 2025).
31. Peña, J.M.; Torres-Sánchez, J.; de Castro, A.I.; Kelly, M.; López-Granados, F. Weed mapping in early-season maize fields using object-based analysis of unmanned aerial vehicle (UAV) images. *PLoS ONE* **2013**, *8*, e77151. https://doi.org/10.1371/journal.pone.0077151
32. Basinger, N.T.; Hestir, E.L.; Jennings, K.M.; Monks, D.W.; Everman, W.J.; Jordan, D.L. Detection of Palmer amaranth (*Amaranthus palmeri*) and large crabgrass (*Digitaria sanguinalis*) with in situ hyperspectral remote sensing. I. Effects of weed density and soybean presence. *Weed Sci.* **2022**, *70*, 198–212. https://doi.org/10.1017/wsc.2021.81
33. Lin, T.-Y.; Maire, M.; Belongie, S.; Hays, J.; Perona, P.; Ramanan, D.; Dollár, P.; Zitnick, C.L. Microsoft COCO: Common objects in context. In *Computer Vision—ECCV 2014*; Fleet, D., Pajdla, T., Schiele, B., Tuytelaars, T., Eds.; Lecture Notes in Computer Science, Vol. 8693; Springer: Cham, Switzerland, 2014; pp. 740–755. https://doi.org/10.1007/978-3-319-10602-1_48
34. QGIS Development Team. *QGIS Geographic Information System*, Version 3.34 (LTR); Open Source Geospatial Foundation Project, 2024. Available online: https://qgis.org (accessed on 5 July 2025).